

## EFFECT OF POST-HYDROTHERMAL TREATMENTS ON THE PHYSICAL PROPERTIES OF ZnO LAYER DERIVED FROM CHEMICAL BATH DEPOSITION

Amalia Sholehah<sup>1,2</sup>, Akhmad Herman Yuwono<sup>1,3\*</sup>, Nofrijon Sofyan<sup>1,3</sup>, Chairul Hudaya<sup>4</sup>,  
Muhammad Ikhlasul Amal<sup>5</sup>

<sup>1</sup>*Department of Metallurgical and Materials Engineering, Faculty of Engineering, Universitas Indonesia, Kampus UI Depok, Depok 16424, Indonesia*

<sup>2</sup>*Department of Metallurgical Engineering, Faculty of Engineering, University of Sultan Ageng Tirtayasa, Jl. Jenderal Sudirman Km 3 Cilegon, Banten 42435, Indonesia*

<sup>3</sup>*Tropical Renewable Energy Center (TREC), Faculty of Engineering, Universitas Indonesia, Kampus UI Depok, Depok 16424, Indonesia*

<sup>4</sup>*Department of Electrical Engineering, Faculty of Engineering, Universitas Indonesia, Kampus UI Depok, Depok 16424, Indonesia*

<sup>5</sup>*Research Centre for Metallurgy and Materials, Indonesian Institute of Science (LIPI), Kawasan Puspiptek Serpong, Banten 42435, Indonesia*

(Received: February 2017 / Revised: March 2017 / Accepted: July 2017)

### ABSTRACT

Among semiconductors, zinc oxide (ZnO) has received great attention due to its wide band-gap and high electron mobility, resulting in various strategic applications. Controlling the physical properties of ZnO is therefore a critical issue in the fabrication of related electronic and optical devices. In this study, ZnO nanorods layers were grown on an ITO glass substrate via chemical bath deposition at low temperature. Prior to the growing process, the layers were deposited using a spin-coating technique. The seeding solution was made by dissolving zinc nitrate tetrahydrate and hexamethylene tetraamine in cold water (0°C) for an hour using a cooler bath. The as-synthesized ZnOs were further subjected to different post-hydrothermal treatment series at a temperature of 150°C for three hours at atmospheric pressure and at 100°C for one hour under one bar of nitrogen gas (N<sub>2</sub>) pressure. The characterization was performed using scanning electron microscopy (SEM), atomic force microscopy (AFM), X-ray diffraction (XRD), and UV-Vis spectroscopy. The SEM results showed that the ZnO nanorods were grown as a vertically aligned hexagonal structure, while the XRD patterns showed a high intensity at the (002) plane. On the basis of investigation, it was found that under post-hydrothermal treatment at 150°C for three hours with atmospheric pressure, the synthesis procedure resulted in nanostructures in the form of ZnO rods. Meanwhile, post-hydrothermal treatment at 100°C for one hour under one bar of nitrogen gas (N<sub>2</sub>) produced ZnO rods and tubes. In general, the post-hydrothermal process provided a high degree of crystallinity. The optimum ZnO layer was obtained after post-hydrothermal treatment at 150°C for three hours at atmospheric pressure, with a crystallite size and band-gap energy of ~18 nm and 3.20 eV, respectively.

**Keywords:** Band-gap energy; Chemical bath deposition; Post-hydrothermal treatments; Crystallite size; ZnO

## 1. INTRODUCTION

Zinc oxide (ZnO) is a versatile semiconductor with very interesting multi-functional properties that can be synthesized easily into various structural forms. As a direct band-gap semiconductor ( $E_g = 3.37$  eV) with a large exciton binding energy (60 meV), ZnO exhibits near UV emission, transparent conductivity, and piezoelectricity. Furthermore, ZnO is a bio-safe and biocompatible material, and thus it can be used for biomedical application without coating (Kenanakis & Katsarakis, 2010; Wu et al., 2011). Two major techniques have been developed for the synthesis of one-dimensional (1D) ZnO arrays, namely, vapor-phase processes and the wet chemical route.

Various vapor-phase processes require expensive and complicated equipment to guarantee suitably rigorous conditions, such as high temperatures ( $\geq 400^\circ\text{C}$ ), low pressures, and adequate atmospheric control, thus limiting the available substrate materials and large-scale production of the arrayed 1D ZnO arrays including nanorods. On the other hand, the wet chemical route is a promising option for large-scale 1D ZnO array fabrication on arbitrary substrates at low cost and under remarkably low temperature conditions (Hu et al., 2010; Wu et al., 2011). Lang et al. (2008) successfully synthesized and characterized ZnO nanorods even at below room temperature. In their work, ZnO nanorods were deposited onto an Si (100) substrate; however, the resulting nanorods were rather random and lacked crystallinity.

The synthesis by chemical bath deposition (CBD) method has generally not been able to produce perfect upright vertical structures above the substrate. In order to improve the physical properties, seed layers were first deposited on the substrate. Meanwhile, post-annealing process application also has a considerable effect on the characteristics of the film, such as the quality of the crystals, electrical properties, as well as the surface morphology (Amoupour et al., 2014). The characteristics of the structure, optical, and electrical properties of the ZnO layer are strongly influenced by the methods and parameters of deposition (Xu et al., 2012). The addition of seeding layers serves as the foundation for the growth of ZnO nanostructures. By adding layers, the surface energy is expected to decline to near zero, and ZnO will grow in the perpendicular direction (Zhang et al., 2013).

In our previous works, it was shown that the annealing temperatures significantly influenced the growth of ZnO nanorods (Sholehah & Yuwono, 2015). In addition, the use of pressure-controlled hydrothermal treatment resulted in an increase in crystallite size while decreasing the band-gap energy (Yuwono et al., 2016). In the current research, ZnO layers were grown on an ITO substrate using an improved CBD technique at low temperature under the influence of external pressures with the addition of nitrogen gas ( $\text{N}_2$ ) into the reactor. The addition of  $\text{N}_2$  gas is expected to produce nanostructured ZnO with better quality in a shorter time. Thus, the risk of structural failure due to post-hydrothermal processes over a long time can be avoided. The results obtained in this work are presented and discussed.

## 2. METHODOLOGY

The seed solution was prepared by dissolving 1:1 equimolar zinc nitrate tetrahydrate ( $\text{Zn}(\text{NO}_3)_2 \cdot 4\text{H}_2\text{O}$ , Merck) and hexamethylene tetraamine ( $\text{C}_6\text{H}_{12}\text{N}_4/\text{HMTA}$ , Merck) 0.05 M in water at  $0^\circ\text{C}$ , which was then allowed to stand for 1 hour in a cooler bath equipped with an automatic temperature controller. Prior to the seed layer deposition, the indium tin oxide ( $\text{InSn}_2\text{O}_3$ , ITO) glass was cleaned in water, acetone, and ethanol with ultrasonic cleaner for 480 seconds in each liquid. Next, the ITO glass was dried and stored in a dry place.

The deposition procedure was adopted from our previous work (Sholehah & Yuwono, 2015). For this purpose, the seed solution was dropped onto the ITO glass and held for 5 minutes to be

absorbed by the surface of the substrate. To remove any remaining unabsorbed solution, spin coating was further carried out, with a speed of 2000 rpm for 5 seconds. The ITO glass that had been coated by the seed solution was further heated at 200°C for 10 minutes. This treatment was carried out 3 times. The ZnO layer on the ITO glass was further grown using the CBD method. The seeded ITO glass was placed vertically in an equimolar Zn-nitrate solution and HMTA 0.05M at 90°C for 3 hours. Furthermore, the ITO glass was washed using distilled water and dried in air. The final result of the CBD synthesized ZnO nanorod layer is termed as **sample A**.

Post-hydrothermal treatment was performed by placing the ITO with the ZnO layer on top of boiling water in a reactor. The ZnO layer was placed upside down, facing the bottom of the reactor. There were two variations of the process undertaken in the experiment. The first variation was carried out using a hydrothermal reactor in a muffle furnace at a temperature of 150°C for 3 hours at atmospheric pressure. This post-hydrothermal treatment is referred to by the acronym **PHT-1**, and the resulting ZnO nanorod layer is coded as **sample B**. In the second variation, the process was carried out in another hydrothermal reactor at 100°C for 1 hour under 1 bar of nitrogen gas (N<sub>2</sub>) pressure. This treatment is hereinafter referred to by the acronym **PHT-2**, and the ZnO nanorod is coded as **sample C**. For each post-hydrothermal process, the collected samples were further washed, dried, and characterized to determine their physical properties.

The morphology of the synthesized ZnO nanorods was examined using scanning electron microscopy (SEM, JEOL JSM-6390A), the crystal structure data was obtained using X-ray diffraction (XRD, Pan Analytical X-Pert Pro), and the optical properties were analyzed using diffuse reflectance (DRS) UV-Vis spectroscopy (Shimadzu 2450). Further confirmation about the nanorod shape and crystallinity was obtained from transmission electron microscope (TEM, Tecnai F20 G<sup>2</sup> 50-200 kV).

### 3. RESULTS AND DISCUSSION

#### 3.1. Morphological Analysis

The morphology and thickness of the ZnO layer were analyzed using SEM and atomic force microscopy (AFM). Figure 1a shows that the seeding layers grown using the CBD process (sample A) appear as sub-micron rod structures of ZnO with an average diameter of 366.16 nm, and they have a fairly good distribution over the substrate. However, the growth direction of the ZnO nanorods is still random and not oriented vertically upright.

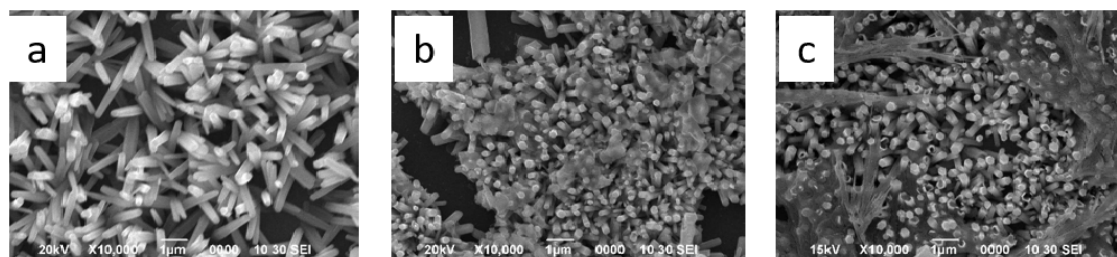


Figure 1 Morphology of ZnO layer on ITO glass after: (a) CBD process (sample A); (b) PHT-1 process (sample B); and (c) PHT-2 process (sample C)

By applying the PHT-1, the size of the ZnO diameter was found to decrease, with an average value of 260.44 nm (sample B). This decrease was due to the separation of nanorods that grew together during the CBD process. By applying the pressure of water vapor, the rods can be separated and oriented to the vertical direction, with a perfect hexagonal shape (Figure 1b).

However, the reaction time was long enough to cause a decrease in the thickness of the ZnO layer. This is due to the partial decay of ZnO, which has been formed and has damage in some parts of the layer. In addition, the water vapor pressure also resulted in a denser layer, as shown in Figure 1b. This resulted in a lower thickness after the PHT-1, as compared to the as-synthesized ZnO layer.

A similar phenomenon was observed in the ZnO layer subjected to PHT-2 treatment (sample C). By this process, the diameter of the nanostructured ZnO decreased by an average value of 306.85 nm. When compared with the PHT-1, the ZnO layer produced by PHT-2 has a better distribution (Figure 1c). The interesting feature in this process is the ZnO layer was not only grown as a rod structure, but at some point it also appeared as a tubular structure. The structure of the film is the flattest and densest when compared with both the previous variations. Data on the diameter and thickness of layers of nanostructured ZnO are presented in Table 1.

Table 1 Average diameter and thickness of ZnO layer

Sample	Average diameter (nm)	Thickness ( $\mu\text{m}$ )
A	366.16	2.04
B	260.44	1.24
C	306.85	1.28

Cross-sectional images of the ZnO layers are presented in Figure 2. In sample A, it is shown that the layers were not vertically arranged, which is correlated with Figure 1a. The as-synthesized ZnO layer was grown in a random direction, with a thickness of 2.04  $\mu\text{m}$ . Applying the post-hydrothermal treatments resulted in denser ZnO layers, as shown in Figures 2b and 2c. In sample B, the layer was treated with PHT-1 and had a thickness of 1.24  $\mu\text{m}$  (Figure 2b). The best layer resulted in sample C, which was treated with PHT-2 and had a thickness of 1.28  $\mu\text{m}$  (Figure 2c).

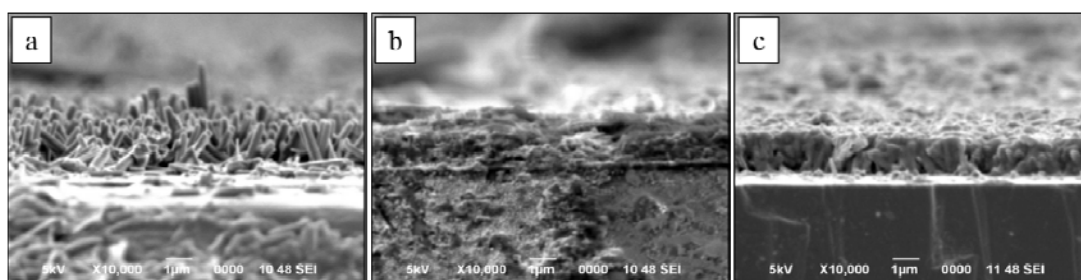


Figure 2 Cross-sectional view of ZnO layer on ITO after: (a) CBD process (sample A); (b) PHT-1 process (sample B); and (c) PHT-2 process (sample C)

The addition of  $\text{N}_2$  gas in the hydrothermal reaction reduced the damage and generated a better ZnO layer. By reducing the reaction time from 3 hours to 1 hour, as well as lowering the reaction temperature from 150°C to 100°C, the risk of ZnO decay becomes smaller. As a result, the obtained layer structure looks more solid and flat, with fewer surface defects.

The grain size in the sample annealed using nitrogen gas (sample C) was greater than the sample annealed with air (sample B). The increase in grain size can be regarded as a trigger of oxygen vacancy in a nitrogen gas environment. The vacancy concentration will increase exponentially as the temperature increases and has an effect on grain growth kinetics by changing the diffusion flux of oxygen vacancies (Amoupour et al., 2014; Ziabari & Ghodsi 2012).

Analysis of the morphology of the ZnO layer using AFM is presented in Figure 3. Two-dimensional (2D) imaging using AFM showed that the as-synthesized ZnO layer appears to grow with an uneven thickness profile (Figure 3a). This is also supported by the corresponding three-dimensional (3D) view. This condition is consistent with the results of the analysis of SEM in Figure 2a, where the ZnO layer after the CBD process still has unoriented direction growth (sample A). This affects the layer thickness profiles, which are then displayed in the form of hills and valleys with a non-uniform height. Application of the PHT-1 resulted in a change in the ZnO layer, with a more uniform profile view (Figure 3b) and corresponding 3D view. In the 3D imaging, it is evident that the ZnO layer has a thickness that is flatter than that from the previous process (sample B). This condition is consistent with the analysis of SEM in Figure 2b, where the ZnO layer after the PHT-1 seemed to have a more uniform thickness compared with the ZnO after the CBD process. The process of PHT-2 also provides better AFM imaging results, as in the SEM analysis (sample C). Figure 3c profiles 2D layers with a thickness that is more equitable, which is supported by its relevant 3D profile. This supports the SEM analysis mentioned previously, which indicates that the ZnO layer on PHT-2 has the best structure (Figure 2c). Simões and his coworkers (2009) found that a sample annealed in a nitrogen gas environment showed an increase in grain size, which implies a reduction in the grain boundary area. The process occurs in the conduction electrons in the conduction band through the grain boundaries. Thus, annealing in a nitrogen gas environment can improve the conductivity of the film.

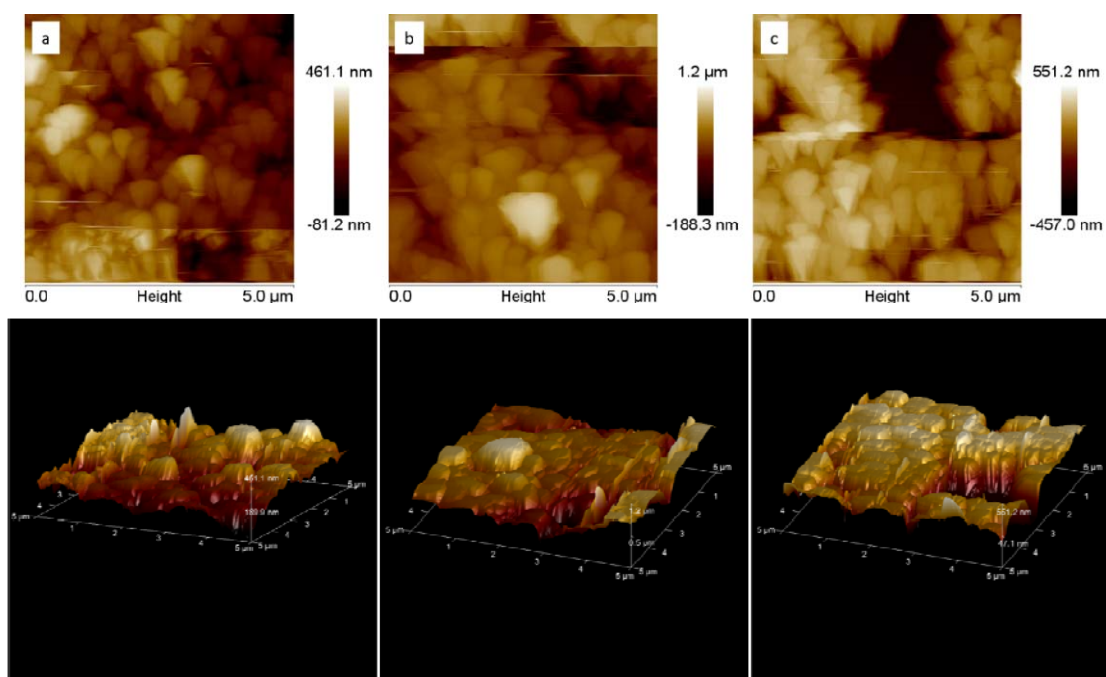


Figure 3 2D AFM images (top) and the corresponding 3D view (bottom) of ZnO on ITO glass after: (a) CBD process (sample A); (b) PHT-1 (sample B); and (c) PHT-2 (sample C)

### 3.2. Structural Analysis

Investigation of the crystal structure of the ZnO layer on the substrate was carried out using XRD, and the results are given in Figure 5. Diffractogram analysis showed that all three samples were identified as ZnO with no reference ICDD 01-078-3322 for sample A, and as no 01-073-8765 for samples B and C. Overall, there are three main peaks with the highest intensity, i.e., at  $20\sim 32^\circ$ ,  $\sim 34^\circ$ , and  $\sim 36^\circ$ . These peaks are correlated with lattice 100, 002, and 101 of the structure of the ZnO wurtzite crystal. In addition, there are also 3 peaks with much

lower intensities of  $20\sim 47$ ,  $\sim 56$ , and  $\sim 63^\circ$ . These correlate with the crystal lattices 102, 110, and 103. The peaks shown at  $2\theta$  diffraction angle of  $20\sim 35^\circ$  are characteristic of ITO glass.

In sample A, it appears that the three dominant peaks have almost the same intensity values (Figure 4a). This indicates that the sample has a random direction of growth, which is consistent with the results of the SEM analysis in Figure 1a. By applying post-hydrothermal treatments (sample B and sample C), the dominant diffraction peaks appear at  $2\theta$  of  $\sim 34^\circ$ , which is characteristic for the lattice (002) (Figures 4b. and 4c). Post-hydrothermal treatments improved the peak structure, resulting in a crystal direction perpendicular to the z-axis. This corresponds to the SEM analysis shown in Figures 1b and 1c.

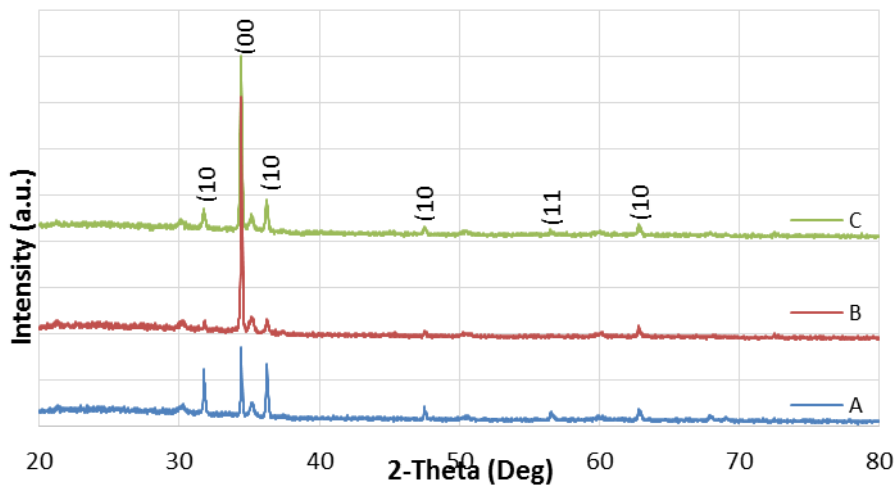


Figure 4 ZnO layer diffractograms after: (a) CBD process (sample A); (b) PHT-1 process (sample B); and (c) PHT-2 process (sample C)

Variations in the post-hydrothermal treatments led to slightly different results in the ZnO layers' diffractograms. In sample B, the peak of the lattice (002) has a very high intensity, far exceeding the other peaks. Thus, in this variation the ZnO layer has only one peak diffractogram (Figure 4b). In sample C, in addition to the peak at lattice (002), there is a small peak intensity of lattice (101) (Figure 4c). Thus, based on the diffractogram generated, it can be concluded that treatment with PHT-1 (sample B) results in the highest crystallinity.

The post-annealing process can have a major impact on the properties of the film formed, such as the quality of the crystals, electrical properties, and surface morphology. Amoupour and his coworkers (2014) demonstrated that samples annealed using nitrogen gas resulted in better crystallinity than samples annealed in air. In addition, electric mobility was increased in the annealing process using nitrogen. Prior to this work, Yuwono et al. (2016) found that pressure-controlled post-hydrothermal treatment led to an increase in crystallite size.

Analysis of the geometric parameters of the nanostructured ZnO layer was carried out by comparing the Scherrer and Williamson–Hall (W–H) methods (Sholehah & Yuwono, 2015). The W–H method is divided into three types of assumptions, namely, the Uniform Deformation Model (UDM), Uniform Deformation Stress Model (UDSM), and Uniform Deformation Energy Density Model (UDEDM). The results are presented in Table 2.

Table 2 Geometrical parameters of ZnO layers

Sample	Scherrer	Williamson Hall (W–H) Method								
	Method	UDM			UDSM			UEDM		
	D (nm)	D (nm)	$\epsilon$ ( $10^{-3}$ )	D (nm)	$\sigma$ (MPa)	$\epsilon$ ( $10^{-3}$ )	D (nm)	$u$ (kJ/m <sup>3</sup> )	$\sigma$ (MPa)	$\epsilon$ ( $10^{-3}$ )
A	15.24	15.24	3.6	23.25	200	1.39	16.72	472	261	1.81
B	17.81	17.81	3	19.05	400	2.70	18.05	602	299	2.01
C	24.94	16.13	3.3	21.43	200	0.33	18.29	420	239	1.76

In the Scherrer method, crystallite size and strain due to the dislocations can be calculated from the peak expansion diffractogram. In order to get an accurate calculation, the effect of the expansion of the peak caused by the interaction of instruments and samples needs to be eliminated first. This can be done using standard materials to determine the peak due to the expansion of the instrument (Prabhu et al., 2013). In this study, the correction of the expansion of the peak due to the effects of instruments was done by reducing the value of the FWHM peak diffractogram measured with standard sample ZnO FWHM values. In the W–H method assuming the UDM, the crystal is considered to be isotropic, where the material properties and strain are considered equal in all directions. Meanwhile, assuming UDSM and UDEDM, the crystal is considered to have anisotropic properties and not to be uniform in all directions (Mote et al., 2012; Khorsand Zak et al., 2011). Scherrer's equation is dependent on any changes to  $1/\cos \theta$ , while the W–H has a dependency on any changes to  $\tan \theta$ . In the W–H method, crystallite size and microstrain occur due to reflection on the widening of the diffraction peaks (Prabhu et al., 2013). The geometric parameters of the ZnO layers are presented in Table 2. Sample B has a value that is relatively more stable than those of other samples. The range of crystallite size values is not very wide ( $\sim 18$ – $19$  nm), and the value of strain ( $\epsilon$ ) ranges between  $2$ – $3 \times 10^{-3}$ . This condition corresponds to Figure 1, which indicates that the ZnO layer with the PHT-1 (sample B) has the highest crystallinity compared to other samples.

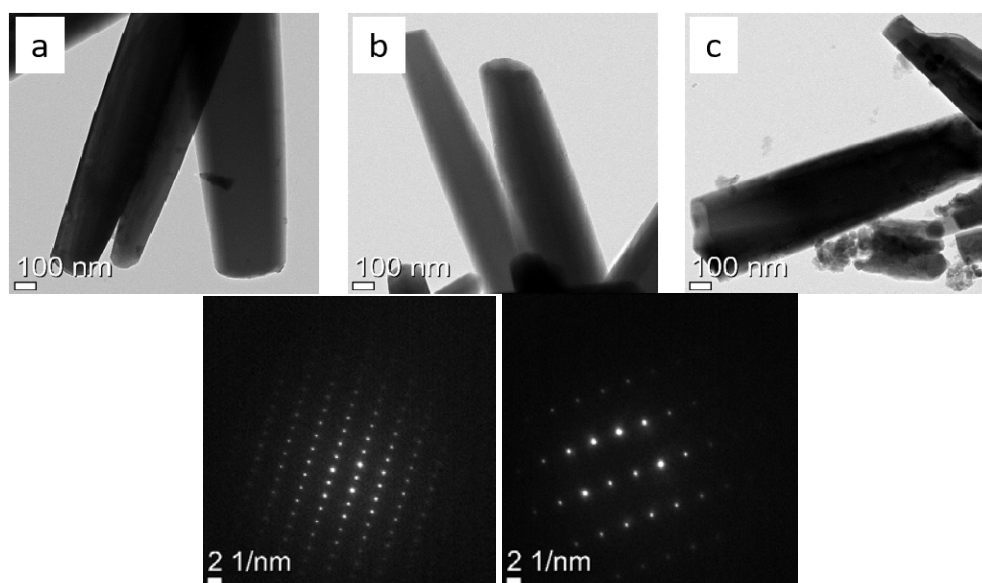


Figure 5 TEM images (top) and the corresponding SAED (bottom) for ZnO nanorods under: (a) CBD process (sample A); (b) PHT-1 process (sample B); and (c) PHT-2 process (sample C)

The images obtained from TEM observation along with the corresponding selected area electron diffraction (SAED) are presented in Figure 5. As seen in Figure 5a, the as-synthesized

ZnO was grown in a nanorod form under CBD treatment. The crystallinity of the structure was good, as shown in the corresponding SAED image. Post-hydrothermal treatments were shown to have a damaging effect on the nanorod structure. As seen in Figure 5b, the nanorods obtained after PHT-1 treatment were slightly smaller compared to the as-synthesized ZnO. With PHT-2 treatment, several small ruptured nanorods were observed in adjacent to large ZnO nanorod structures. However, the crystallinity of the ZnO nanorods was still well maintained, as observed in the corresponding SAED images b and c.

### 3.3. Optical Analysis

One of the optical properties identified in this study is the band-gap energy ( $E_g$ ). Figure 6 presents the band-gap energy values of the ZnO nanorods samples. The calculated  $E_g$  value for sample A is 3.25 eV. Samples B and C have lower  $E_g$  values (i.e., 3.20 eV), respectively. The lower  $E_g$  value is correlated to the crystallite size, which has been described earlier. Samples B and C have a greater crystallite size when compared to sample A, which results in the low  $E_g$  values in the calculations.

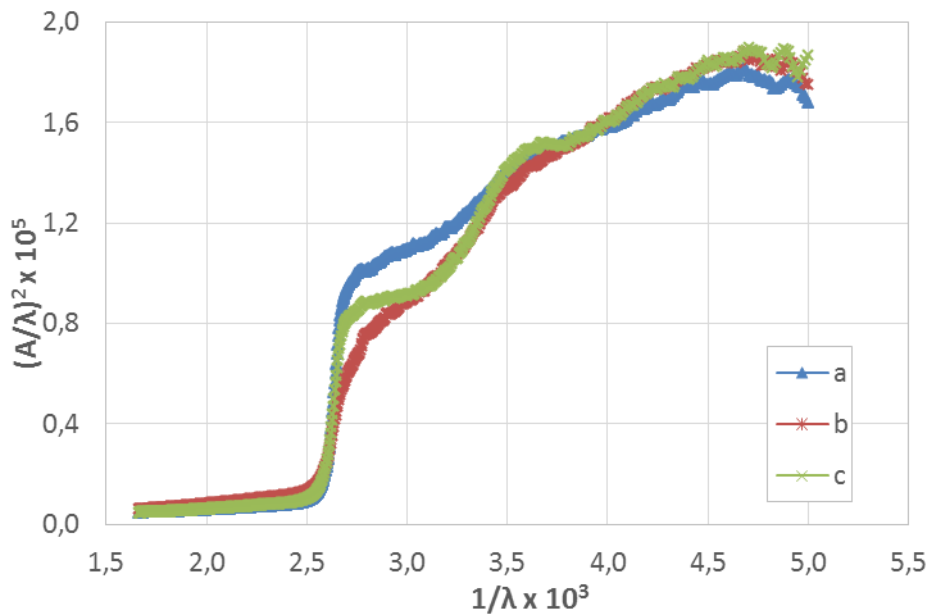


Figure 6  $E_g$  determination using ASF plot for ZnO layers after: (a) CBD process (sample A); (b) PHT-1 process (sample B); and (c) PHT-2 process (sample C)

Various treatment processes were used in the experiment to produce nanostructures with different characteristics. One of the parameters that is greatly affected by the synthesis process is the crystallite size. This parameter has a great dependence on the temperature. Generally, a large crystallite size is obtained by raising the reaction temperature. However, in this experiment, the role of temperature was replaced by pressure. The crystallite size has a strong correlation with the  $E_g$  value, which will decline if the crystallite size increases. Thus, for each treatment process in the synthesis of nanostructured ZnO, the  $E_g$  value will be correlated with the changes in the crystallite size of the structures.

From the experiments, it also appears that the tail energy ( $E_u$ ) trend has a value that is inversely proportional to  $E_g$  (Ziabari & Ghodsi, 2012). The  $E_u$  value showed an exponential tail that appears as the amorphous nature of the material (Ikhmayies & Ahmad-Bitar, 2013). The  $E_u$  profiles for the ZnO nanorod samples are presented in Figure 7. These values correlate with the

optical transitions between localized states adjacent to the valence and conduction bands' extended state (Rusdi et al., 2011; Mote et al., 2012). The optical properties of the samples in the forms of  $E_g$  and  $E_u$  are summarized in Table 3.

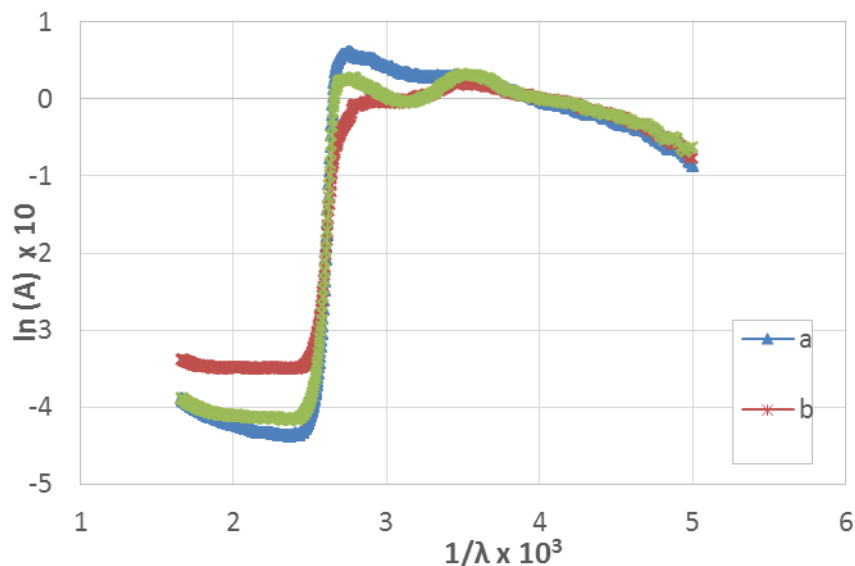


Figure 7  $E_u$  determination using ASF plot for ZnO layers after: (a) CBD process (sample A); (b) PHT-1 process (sample B); and (c) PHT-2 process (sample C)

Table 3 Band-gap ( $E_g$ ) and Urbach ( $E_u$ ) energy of ZnO layers

Sample	$E_g$ (eV)	$E_u$ (eV)
A	3.25	0.19
B	3.20	0.34
C	3.20	0.21

#### 4. CONCLUSION

ZnO nanostructures layers have been successfully synthesized using CBD and post-hydrothermal methods. Prior to the growing process, a seed layer was attached to an ITO glass substrate using a spin-coating technique. The seed layer increased the stability of the ZnO nanostructure layers. Differences in post-hydrothermal conditions resulted in the growth of nanostructures with different shapes. Using the PHT-1, the synthesis resulted in ZnO rods, while the PHT-2 produced ZnO rods and tubes. In general, the post-hydrothermal process was able to provide a high degree of crystallinity. The optimum ZnO layer was obtained after the PHT-1 process with a crystallite size and band-gap energy of ~18 nm and 3.20 eV, respectively. The obtained ZnO nanorods in this work are promising for applications in several electronic and photonic devices, with further adjustments.

#### 5. ACKNOWLEDGEMENT

The authors would like to thank the Ministry of Research and Higher Education of the Republic of Indonesia for funding this research through Hibah PUPT DIKTI 2016 No. 1141/UN2.R12/HKP.05.00/2016.

## 6. REFERENCES

- Amoumpour, E., Ziabari, A.A., Andarva, H., Ghodsi, F.E., 2014. Influence of Air/N<sub>2</sub> Treatment on the Structural, Morphological and Optoelectronic Traits of Nanostructured ZnO: Mn Thin Films. *Superlattices and Microstructures*, Volume 65, pp. 332–343
- Hu, S.-H., Chen, Y.-C., Hwang, C.-C., Peng, C.-H., Gong, D.-C., 2010. Development of a Wet Chemical Method for the Synthesis of Arrayed ZnO Nanorods. *Journal of Alloys and Compounds*, Volume 500(2), pp. L17–L21
- Ikhmayies, S.J., Ahmad-Bitar, R.N., 2013. A Study of the Optical Bandgap Energy and Urbach Tail of Spray-deposited CdS:In Thin Films. *Journal of Material Research and Technology*, Volume 2(3), pp. 221–227
- Kenanakis, G., Katsarakis, N., 2010. Light-induced Photocatalytic Degradation of Stearic Acid by C-axis Oriented ZnO Nanowires. *Applied Catalysis A: General*, Volume 378(2), pp. 227–233
- Khorsand Zak, A., Abd. Majid, W.H., Abrishami, M.E., Yousefi, R., 2011. X-ray Analysis of ZnO Nanoparticles by Williamson–Hall and Size–Strain Plot Methods. *Solid State Sciences*, Volume 13(1), pp. 251–256
- Lang, J., Yang, J., Li, C., Yang, L., Han, Q., Zhang, Y., Wang, D., Gao, M., Liu, X., 2008. Synthesis and Optical Properties of ZnO Nanorods. *Crystal Research and Technology*, Volume 43(12), pp. 1314–1317
- Mote, V.D., Purushotham, Y., Dole, B.N., 2012. Williamson–Hall Analysis in Estimation of Lattice Strain in Nanometer-sized ZnO Particles. *Journal of Theoretical and Applied Physics*, Volume 6(1), pp. 1–8
- Prabhu, Y.T., Rao, K.V., Sai Kumar, V.S., Kumari, B.S., 2013. X-ray Analysis of Fe Doped ZnO Nanoparticles by Williamson–Hall and Size–Strain Plot. *International Journal of Engineering and Advanced Technology*, Volume 2(4), pp. 268–274
- Rusdi, R., Abd Rahman, A., Mohamed, N.S., Kamarudin, N., Kamarulzaman, N., 2011. Preparation and Band Gap Energies of ZnO Nanotubes, Nanorods and Spherical Nanostructures. *Powder Technology*, Volume 210(1), pp. 18–22
- Sholehah, A., Yuwono, A.H., 2015. Stress–Strain Analysis on ZnO Nanostructures Synthesized via Wet Chemistry Method. *Advanced Materials Research*, Volume 1112, pp. 57–61
- Sholehah, A., Yuwono, A.H., 2015. The Effects of Annealing Temperature and Seed Layer on the Growth of ZnO Nanorods in a Chemical Bath Deposition Process. *International Journal of Technology*, Volume 6(4), pp. 565–572
- Simoes, A.Z., Riccardi, C.S., Dos Santos, M.L., Garcia, F.G., Longo, E., Varela, J.A., 2009. Effect of Annealing Atmosphere on Phase Formation and Electrical Characteristics of Bismuth Ferrite Thin Films. *Material Research Bulletin*, Volume 44(8), pp. 1747–1752
- Wu, X., Chen, H., Gong, L., Qu, F., Zheng, Y., 2011. Low Temperature Growth and Properties of ZnO Nanorod Arrays. *Advances in Natural Sciences: Nanoscience and Nanotechnology*, Volume 2(3), pp. 1–4
- Xu, L., Zheng, G., Miao, J., Xian, F., 2012. Dependence of Structural and Optical Properties of Sol–Gel Derived ZnO Thin Films on Sol Concentration. *Applied Surface Science*, Volume 258(19), pp. 7760–7765
- Yuwono, A.H., Kurniawan, D., Sofyan, N., Ramahdita, G., Sholehah, A., 2016. Effect of Pressure in Post-Hydrothermal Treatment on the Nanostructural Characteristics of ZnO Nanoparticles. *International Journal of Technology*, Volume 7(3), pp. 424–430
- Zhang, R.H., Slamovich, E.B., Handwerker, C.A., 2013. Controlling Growth Rate Anisotropy for Formation of Continuous ZnO Thin Films from Seeded Substrates. *Nanotechnology*, Volume 24, pp. 195603–195610

Ziabari, A.A., Ghodsi, F.E., 2012. Growth, Characterization and Studying of Sol–Gel Derived CdS Nanocrystalline Thin Films Incorporated in Polyethylene Glycol: Effects of Post-heat Treatment. *Solar Energy Materials and Solar Cells*, Volume 105, pp. 249–262